J Mater Sci (2010) 45:652–661
DOI 10.1007/s10853-009-3979-5

Mechanical behavior of A265 single fibers

Jaeyoung Lim · James Q. Zheng · Karl Masters · Weinong W. Chen

Received: 19 June 2009 / Accepted: 12 October 2009 / Published online: 30 October 2009

Abstract The mechanical behavior of A265 high-performance fibers was experimentally investigated at both low and high strain rates. Axial, transverse, and torsional experiments were performed to measure the five material constants on a single fiber assumed as a linear, transversely isotropic material. In order to determine the tensile response of the fiber at high rates, a modified Kolsky tensile bar, also known as a split Hopkinson tension bar (SHTB) for single-fiber tests, was used. The diameter of each fiber was measured individually using a high-resolution scanning electron microscope for accurate stress calculation. A pulse shaper technique was adopted to generate a smooth and constant-amplitude incident pulse to produce deformation in the fiber specimen at a nearly constant strain rate. The tensile strength of the fiber exhibits both rate and gage-length effects.

Introduction

High-performance fibers with high strength, light weight, and high-temperature stability have been developed for increasing demands in body and vehicle armors. In order to develop predictive capabilities of impact events involving high-performance fibers, it is critical to understand the performance of single filaments during impact. Determination of the mechanical properties at both low and high strain rates is an integral aspect of the understanding development.

J. Lim · W. W. Chen (✉)
Schools of Aeronautics/Astronautics and Materials Engineering, Purdue University, West Lafayette, IN 47907-2045, USA
e-mail: wchen@purdue.edu

J. Q. Zheng · K. Masters
US Army PM-Soldier Equipment, Haymarket, VA 20169, USA

High-performance fibers are typically very strong under axial tension but much weaker in the transverse directions [1, 2]. There have been research efforts on the mechanical behavior of high-performance fabrics or fiber bundles at high strain rates [3–6]. Shim et al. [4] have observed that Twaron® fabrics, similar to the commonly known Kevlar®, are highly strain-rate dependent. In their experimental results, both the tensile strength and modulus increase with increasing strain rates while the failure strains decrease. The phenomenon was related to the ductile–brittle transition at high strain rates. More recently, Languerand et al. [6] investigated the tensile behavior and failure mechanisms of PPTA fiber bundles at high strain rates using a conventional tension Kolsky bar and showed insignificant strain-rate effects on the elastic modulus in PPTA fiber bundles. For a single fiber deforming at high strain rates, few experimental results are available despite the obvious importance of this behavior in the understanding of impact response of flexible armors. Cheng et al. [7] observed insignificant loading-rate effects on the tensile behavior of Kevlar® KM2 single fibers at both quasi-static and high strain rates. In addition to longitudinal strength and Young's modulus, other experiments have also been reported for other mechanical properties such as transverse compression behavior [8–10] and longitudinal shear behavior [11]. Despite these research efforts, the documented experimental results on the high-rate behavior of high-performance fibers are still very limited.

In this study, we examined the mechanical behaviors of a single A265 fiber at both quasi-static and high strain rates. The five elastic constants of transversely isotropic material were determined by adopting three different types of experiments. The strain-rate effects and gage-length effects on the axial tensile strength of the A265 fiber were also investigated. A modified Kolsky tension bar was used to

conduct the dynamic tension experiments at the strain rate of $\dot{\varepsilon} \approx 1000\ s^{-1}$. The quasi-static experiments were performed with a conventional material testing system (MTS).

Experimental procedure and results

Materials

The material is a high-performance A265 "Termotex" single fiber, which is a 29.4 tex co-polymer aramid Rusar fiber containing 5-amino-2-(*p*-amino phenyl)-benzimidazole or related monomers. It has a density of 1450 kg/m^3. A high-resolution scanning electron microscope (SEM) image of such a fiber is shown in Fig. 1. The average fiber diameter measured from 15 fibers is 9.28 ± 0.17 μm.

Quasi-static elastic constants of the fiber

In terms of modeling their constitutive behavior, these fibers may be regarded as linearly elastic, transversely isotropic, and homogeneous [2]. The elastic response of such materials is described by five independent material constants which are coordinate dependent. Consider the single fiber in Cartesian coordinate system with the x_3 axis as the axis of transverse isotropy shown in Fig. 2, the stress–strain relationships for a linear, transversely isotropic material are expressed as:

$$\begin{Bmatrix} \varepsilon_{11} \\ \varepsilon_{22} \\ \varepsilon_{33} \\ \varepsilon_{23} \\ \varepsilon_{31} \\ \varepsilon_{12} \end{Bmatrix} = \begin{bmatrix} S_{11} & S_{12} & S_{13} & 0 & 0 & 0 \\ S_{12} & S_{11} & S_{13} & 0 & 0 & 0 \\ S_{13} & S_{13} & S_{33} & 0 & 0 & 0 \\ 0 & 0 & 0 & 0.5S_{44} & 0 & 0 \\ 0 & 0 & 0 & 0 & 0.5S_{44} & 0 \\ 0 & 0 & 0 & 0 & 0 & S_{11}-S_{12} \end{bmatrix} \begin{Bmatrix} \sigma_{11} \\ \sigma_{22} \\ \sigma_{33} \\ \sigma_{23} \\ \sigma_{31} \\ \sigma_{12} \end{Bmatrix} \tag{1}$$

where the five independent compliance constants S_{ij} can be expressed in terms of elastic constants as:

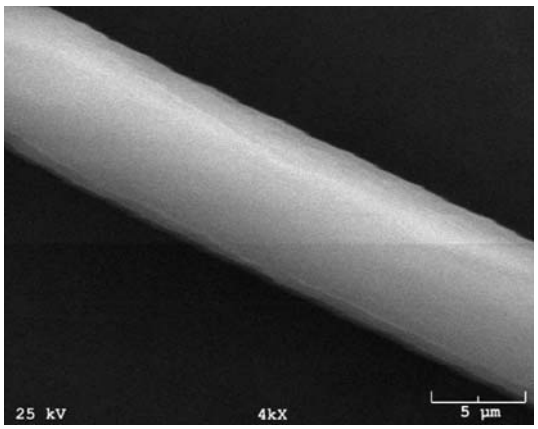

Fig. 1 High-resolution SEM image of an A265 single fiber

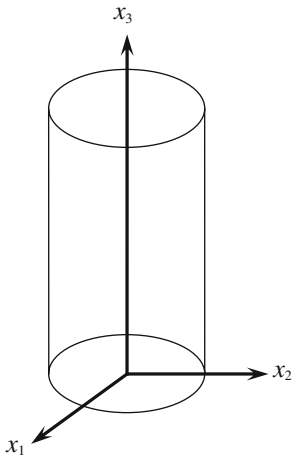

Fig. 2 Geometry of a single fiber model in Cartesian coordinates

$$S_{11} = \frac{1}{E_1},\ S_{12} = -\frac{v_{12}}{E_1},\ S_{13} = -\frac{v_{13}}{E_1} = -\frac{v_{31}}{E_3},\ S_{33} = \frac{1}{E_3},$$
$$S_{44} = \frac{1}{G_{13}} \tag{2}$$

where E_1 is the transverse modulus; E_3 is the longitudinal modulus; G_{13} is the longitudinal shear modulus; and v_{12} and v_{31} are the transverse and the longitudinal Poisson's ratios, respectively. In order to determine the five mechanical constants of the A265 single fiber, we used three different types of experiments in this study, as briefly described below.

Axial tension experiments

The quasi-static axial tension experiments are performed according to the ASTM standard test method for tensile strength and Young's Modulus of fibers (C1577-03). This standard technique is a mounting method used for very fine specimens. A rectangular construction paper is used as the template for a single fiber due to its relatively high stiffness. A circular hole is cut in this template, and then a fiber specimen is glued across this circular hole. The gage length of the fiber is the distance between the glue joints on either side of the circular hole. The template is connected to MTS for axial loading through a set of special grips.

Figure 3 shows the tensile experimental results at a quasi-static strain rate of 0.001 s^{-1}. Only about half of the 15 repeated experiments are shown for the purpose of clarity. The results in Fig. 3 show that the tensile stress–strain behavior of the single fiber at a gage length of 10 mm is reasonably linearly elastic. There are variations in failure stresses and failure strains, but the elastic modulus is consistent from experiment to experiment. The longitudinal Young's modulus, E_3, of A265 fiber is measured to be 140.51 ± 2.32 GPa with 95% confidence

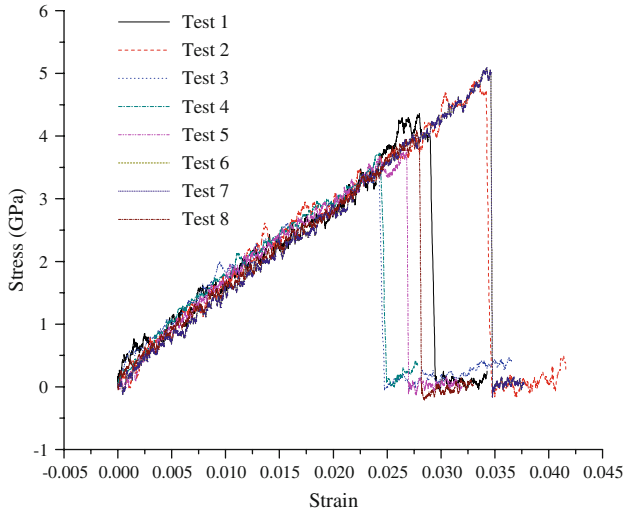

Fig. 3 Tensile experimental results at a strain rate of 0.001 s^{-1} (Gage length = 10 mm)

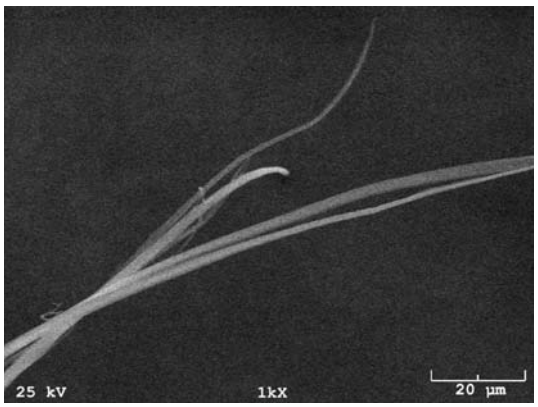

Fig. 4 High-resolution SEM image of a failed end of an A265 single fiber

interval from the results of 15 repeated tests. The ultimate strength and failure strain are 4.28 ± 0.33 GPa and 3.05 ± 0.25%, respectively.

Figure 4 shows a high-resolution SEM image of the failed end of an A265 single fiber. Fibrillation is clearly shown on the failed end. The structure of most common fibers has been analyzed and characterized as anisotropic, which gives higher strength and modulus in the fiber longitudinal direction than in the transverse direction [1, 2]. The weak lateral interactions in fiber facilitate the fibrillation [2], which has profound effects on the tensile failure mechanisms, as indicated by the failure mode shown in Fig. 4.

Gage-length effects In addition to the tensile experiments performed on single fiber samples with a gage length of 10 mm, quasi-static tensile experiments are also performed at four other gage lengths of 2.5, 5.5, 50, and 100 mm to investigate the gage-length effects on the tensile strength. All the experiments are performed at the same quasi-static strain rate of 0.001 s^{-1}. The gage-length effect may provide a measure of the defect distribution along the length of the fiber. A significant defect will limit the tensile strength as measured. The experimentally determined values of the tensile strengths of A265 fibers with different gage lengths are summarized in Table 1. At each gage length, 15 tests are repeated. The results listed in Table 1 are with 95% confidence interval as obtained from the 15 repeated experiments.

The experimental results show that the ultimate tensile strength of a single A265 fiber depends on the gage length, especially over the small gage length of below 10 mm, as shown in Fig. 5. The tensile strength increases with decreasing gage length. Similar observations have been reported on other fibers [12, 13], although our own measurements showed insignificant effects of the gage length on the tensile strength of some Kevlar® fibers over the same length changes. The gage-length effects on the A265 fiber also become insignificant when the gage length is increased beyond 10 mm, which is also shown in Fig. 5. This experimentally measured trend indicates that, for this specific fiber, a strength-limiting defect is very likely to exist in the fiber with a length of at least 10 mm.

Compliance correction During a quasi-static test of a single fiber with high modulus, especially when the gage length is small (below 5 mm), the system compliance must be considered for the accurate determination of strain

Table 1 Longitudinal mechanical properties of A265 fiber deforming at quasi-static rates

Gage length l (mm)	Tenacity (g/denier)	Failure load (N)	Ultimate strength (GPa)	Failure strain (%)	Young's modulus (GPa)
2.5	42.52	0.36 ± 0.02	5.40 ± 0.26	5.79 ± 0.28	91.39 ± 4.96
5.5	38.19	0.33 ± 0.03	4.85 ± 0.35	3.63 ± 0.28	126.66 ± 5.08
10	33.70	0.29 ± 0.02	4.28 ± 0.33	3.05 ± 0.25	140.51 ± 2.32
50	32.99	0.28 ± 0.01	4.19 ± 0.12	2.77 ± 0.13	151.06 ± 3.98
100	31.65	0.27 ± 0.01	4.02 ± 0.15	2.56 ± 0.15	156.72 ± 3.33

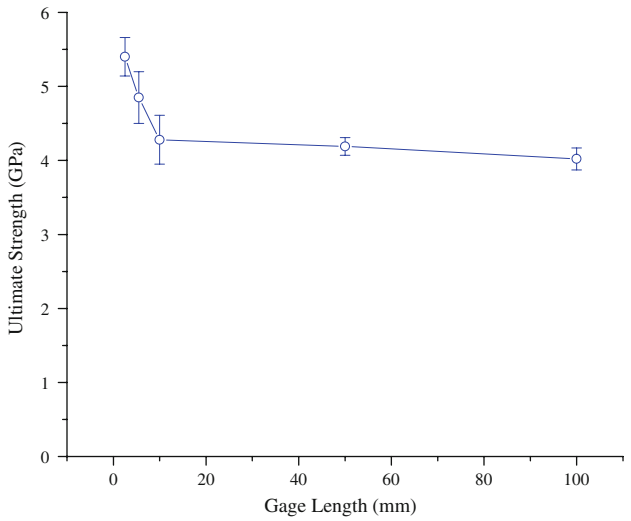

Fig. 5 Variation of the ultimate strength of A265 fibers over the gage length

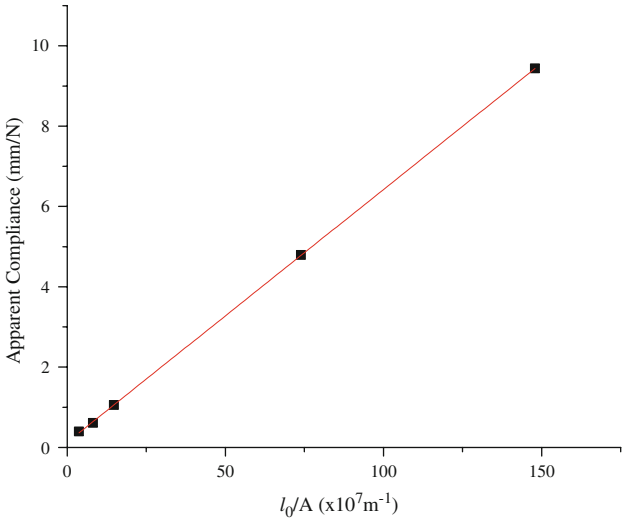

Fig. 6 Apparent compliance versus gage length divided by fiber cross-sectional area

and Young's modulus, as outlined in ASTM test method C 1577-03/Reapproved 2008. For a given material, the effects of the system compliance, which is dependent on the testing machine and its grip system, decrease as the gage length increases [14, 15]. In the case where the strain is not measured directly on the gage section of the specimen, the actual specimen elongation and fiber Young's modulus can be determined by correcting the system compliance. For instance, the elongation at a gage length of 2.5 mm is only 0.145 mm. This result is comparable to the elongation due to the system compliance, and thus, must be corrected.

The procedure to calculate the system compliance is described in ASTM C1577-03. In the study reported in this article, tensile tests of single fibers are performed at five different gage lengths as summarized in Table 1. The system compliance can be determined by plotting $\Delta L/F$ (C_a, *Apparent Compliance*) versus l_0/A curve in which ΔL is the cross-head displacement measured from the tested system, F is the force at failure, A is the fiber cross-sectional area, and l_0 is the gage length. In Fig. 6, the intercept to zero gage length indicates the value of the system compliance, C_s, which is 0.13 mm/N.

The system compliance-corrected elongation to break and Young's modulus are given by:

$$\varepsilon_{\text{Corrected}} = \frac{\Delta L - C_s F}{l_0}$$
$$E_{\text{Corrected}} = \frac{l_0}{A(C_a - C_s)} \quad (3)$$

Figures 7 and 8 show the variations of the uncorrected and corrected elongation to break and Young's modulus over the gage length, respectively. The error between the uncorrected and corrected values in strain to failure and

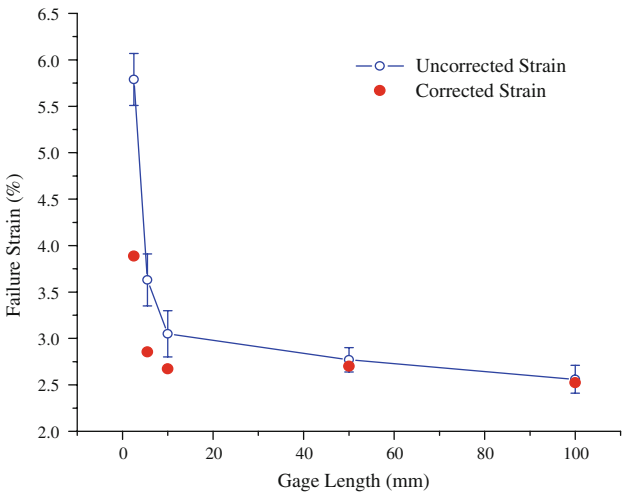

Fig. 7 Variations of the uncorrected and corrected elongation to break along the gage length

Young's modulus decreases as the gage length increases. In the range of the gage length over 10 mm, a gage-length-independent value can be determined. The failure strain and Young's modulus in long samples are 2.73% and 159.78 GPa, respectively. These results demonstrate that the system compliance correction is needed in data reduction for determining accurate elongation to break and Young's modulus, especially for high modulus fibers at short gage lengths.

Transverse compression experiments

An experimental setup is modified to investigate the transverse mechanical behavior of a single A265 high-performance fiber. The schematic diagram for measurement of the

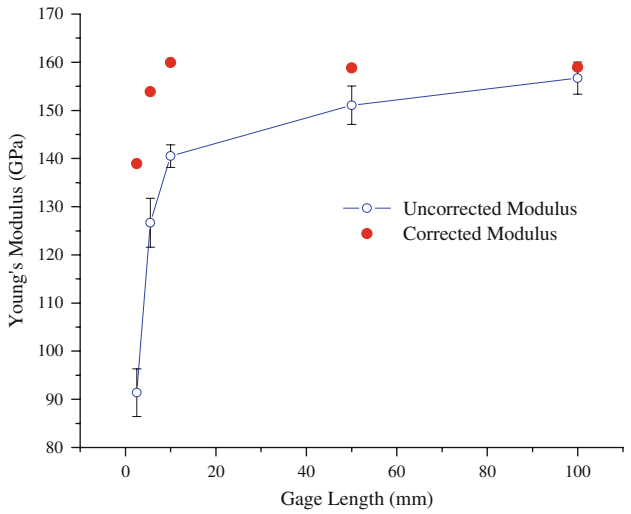

Fig. 8 Variations of the uncorrected and corrected Young's modulus along the gage length

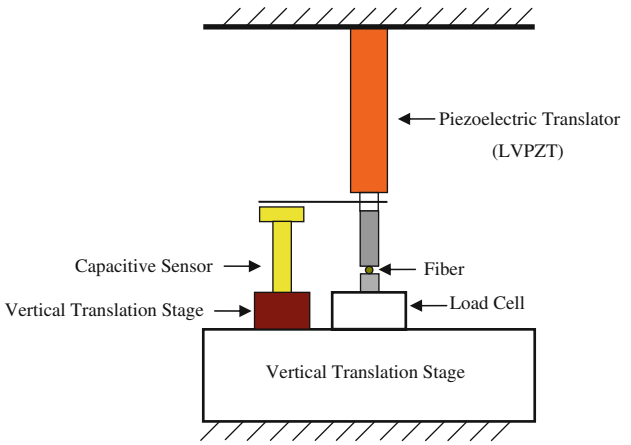

Fig. 9 A schematic diagram of the transverse test system

force and displacement applied to the single fiber transversely is shown in Fig. 9. The system includes a piezoelectric translator (Physik Instrument LVPZT, P840.20) traveling up to 30 μm, push and supporting rods, and a precision vertical translation stage for the proper positioning and alignment. Transverse compressive loading and displacement are measured directly by a low profile load cell with a capacity of 22.24 N (5 lbf) and a capacitive displacement sensor with sub-nanometer resolution (Physik Instrument D510.100), respectively.

The transverse modulus of a single fiber from the compression experiments can be obtained through an analytical solution with measurements of Poisson's ratios and longitudinal modulus. The contact problem of spherically or cylindrically isotropic elastic bodies has been investigated by many researchers [7–10, 16–18]. Hardley et al. [16] derived the analytical solution for the width of the contact zone when a fiber is compressed between two parallel rigid plates. Pinnock et al. [17] extended the study to derive an analytical solution for the diameter of a fiber in terms of the elastic constants and applied load. Phoenix et al. [18] extended the solution of this problem to a linearly elastic, transversely homogeneous orthotropic cylinder. Recently, Cheng et al. [7, 10] derived the relations between the measurable quantities of the transverse compression loader: applied force and displacement, and the transverse modulus of a single fiber.

The problem may be considered as the case of plane strain since the contact width is small compared with the axial dimension of the fiber. This problem is schematically illustrated in Fig. 10. In this article, the relations between displacement and applied load based on the Hertz and McEwen's solution [19] are introduced. After normalizing the compressive load and the displacement by the diameter of the fiber, the equation is as follows [16, 17]:

$$\bar{U} = \frac{4\bar{\sigma}}{\pi b^2}\left[\left(-\frac{v_{12}}{E_1} - \frac{v_{31}^2}{E_3}\right)\left(\sqrt{b^2 + r^2} - r\right)r + \left(\frac{1}{E_1} - \frac{v_{31}^2}{E_3}\right)b^2 \ln\frac{\sqrt{b^2 + r^2} + r}{b}\right] \tag{4}$$

where b is given by:

$$b = \sqrt{\frac{8\bar{\sigma}r}{\pi}\left(\frac{1}{E_1} - \frac{v_{31}^2}{E_3}\right)} \tag{5}$$

where E_1 and E_3 are transverse and longitudinal Young's modulus, respectively, which are constant within small deformation. v_{12} and v_{31} are the transverse and longitudinal Poisson's ratios, respectively. b is one half of the width of the contact zone. r is the radius of the fiber specimen. F stands for the transverse compressive load per unit length along the fiber axial direction, and δ is the transverse displacement. Finally, $\bar{\sigma}$ and $\bar{U}$ are the nominal compressive stress and nominal compressive strain, respectively.

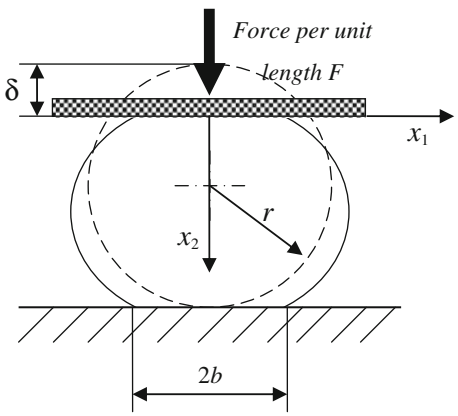

Fig. 10 Transverse compression of a single fiber

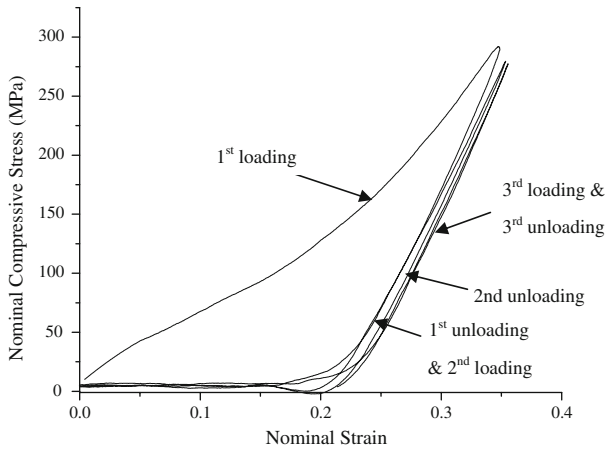

Fig. 11 Transverse compressive behavior of an A265 single fiber

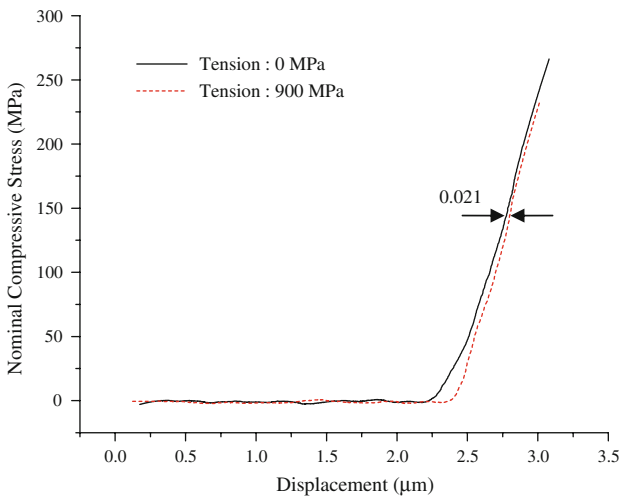

Fig. 12 Estimation of the extensional Poisson's ratio of an A265 single fiber

Experimental results of typical consecutive loading and unloading cycles with constant deformation rate on a fiber specimen from a virgin state are shown in Fig. 11. The results show that the transverse response of the fiber has a similar behavior as the Mullin's effects in rubber mechanics. The first loading cycle caused a large residual strain up to 0.2 in terms of nominal strain in the material that led to significantly different behavior in the follow-up loading cycles.

Estimation of the longitudinal Poisson's ratio The longitudinal Poisson's ratio, v_{31}, needs to be determined to estimate the transverse modulus of a single fiber from the transverse compression experiments. Pinnock et al. [17] determined the longitudinal Poisson's ratio by measuring the diameter and length changes in fiber under longitudinal tension. These direct measurements were performed under constant strain for the convenience to measure the longitudinal length changes. In this study, we adopt the estimation method of Poisson's ratio used by Cheng et al. [10].

Two consecutive transverse compression tests are performed at two different locations in the same single fiber. First, compression test is conducted in a fiber without axial tension, and, then, a second test is performed with a longitudinal pre-tension of 0.9 GPa at a new location 5 mm away from the first loading spot. The shift in displacement from the data represents the diameter change in the single fiber due to the applied longitudinal tension. The results from such a suite of two tests are shown in Fig. 12. Since the A265 fiber has a very consistent diameter as measured earlier, the experimental result on v_{31} is considered reliable.

The Poisson's ratio, v_{31}, defined as the ratio of the transverse strain normal to the applied load divided by the longitudinal strain in the direction of the applied load, can be expressed as

$$v_{31} = -\frac{E_3}{\sigma_3}\varepsilon_1 = -\frac{E_3}{\sigma_3}\frac{\Delta D}{D} \tag{6}$$

where ΔD is the diameter change in transverse direction. The measured diameter change from the results shown in Fig. 12 is 0.021 μm. From Eq. 6, the longitudinal Poisson's ratio is calculated as 0.402.

The transverse Poisson's ratio, v_{12}, also should be determined to estimate the transverse Young's modulus. Since our current experimental setup is unable to measure this value, we assumed the value to be 0.4 based on the curve fitting results from the transverse experimental data and theoretical prediction.

Estimation of the transverse Young's modulus The transverse Young's modulus E_1 of A265 single fibers is determined by matching the nominal compressive stress and nominal strain curves obtained from experiments and from analytical modeling with the modulus as parameter. The stress–strain curves of A265 fibers from the transverse compression tests and theoretical solutions derived in Eqs. 4–6 are compared in Fig. 13. The results show that the transverse Young's modulus is 1.83 GPa from Eqs. 4 and 5. The theoretical predictions for the transverse compressive behavior agree well with experimental measurements at small strains of <5%, as shown in Fig. 13. When the strains become large, the fiber exhibits nonlinear behavior that deviates from the assumptions for the analytical solution. The theoretical analysis also assumes a circular cross section of the fiber which is no longer true at large strains.

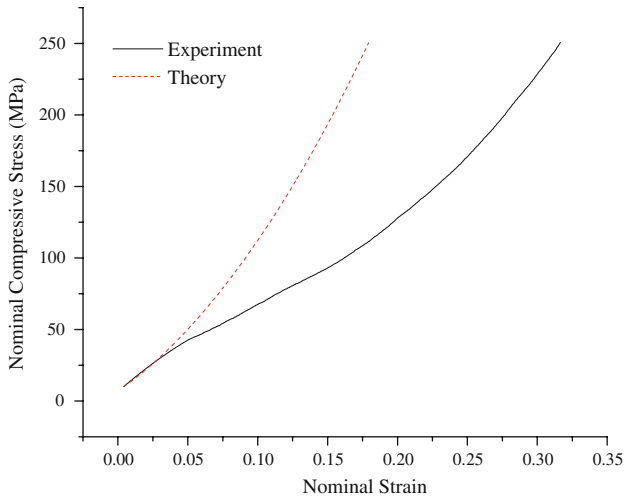

Fig. 13 Comparison between model prediction and experimental data of an A265 single fiber

Torsional shear experiments

In order to determine the longitudinal shear modulus of an A265 single fiber, we used a technique originally developed by Tsai and Daniel [11]. Figure 14 shows the schematic diagram of a torsional pendulum system. A length of fiber is suspended at one end, and a nylon washer with a mass is attached at the other end of the fiber. Assume the fiber to be linearly elastic, transversely isotropic, and homogeneous. The longitudinal shear modulus can be derived in terms of the frequency of oscillation and the geometry of the system:

$$G_{13} = \frac{\pi M\left[8\left(D_o^2 - D_i^2\right) + \frac{32}{3}h^2\right]lf^2}{d^4} \tag{7}$$

where M is the mass of the washer, D_o and D_i are the outer and inner diameters of the nylon washer, respectively; h is the thickness of the nylon washer; l is the length of the fiber; f is the oscillation frequency of the torsional pendulum, and d is the diameter of the fiber.

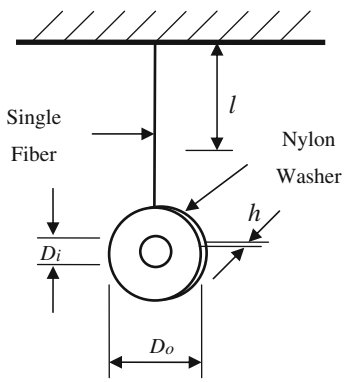

Fig. 14 Schematic diagram of a torsional pendulum

Table 2 Longitudinal shear modulus of A265 fibers

Specimen no.	Length l (mm)	Frequency f (s^{-1})	Diameter d (μm)	Shear modulus G_{13} (GPa)
1	2.02	0.223	9.54	10.85
2	2.02	0.220	9.08	12.87
3	2.44	0.208	9.12	13.65
4	2.05	0.211	9.34	10.73

A nylon washer with a mass of 0.560 g, of 7.94 mm (5/16 in.) outer diameter (D_o), of 3.56 mm (0.14 in.) inner diameter (D_i), and of 3.15 mm (0.134 in.) thickness (h) is used as the mass of the torsional pendulum. A length of fiber is selected within 3.0 mm to avoid the high damping effect in long fibers. The experimental results are tabulated in Table 2. The longitudinal shear modulus of the A265 fiber calculated from the experimental data is 12.03 ± 0.78 GPa.

Tensile behavior at high strain rates

A miniaturized tension bar

In order to determine the tensile response of the fiber at high rates, we modified a Kolsky tensile bar, which is also known as a split Hopkinson tension bar (SHTB), for single-fiber experiments. The concept of Kolsky bar, first introduced by Kolsky [20] in 1949 for compression experiments, has been widely used to determine the dynamic stress–strain relations of materials under dynamic loading at high strain rates [21, 22]. Owing to the small size of the specimen investigated in this study, we used a miniature version of a tension bar, which is shown in Fig. 15. The miniature tension bar consists of an incident bar with a flange, a fiber specimen, and a load cell. The incident bar is made of an aluminum-alloy rod with a diameter of 6.35 mm (0.25 in.) and a length of 1651 mm (65 in.). The impact tube of aluminum with a length of 101.6 mm (4 in.) is free to slide on the outer surface of a brass tube. This brass tube separates the incident bar and the striker tube. This separation is necessary to minimize the noise caused by the sliding of striker tube that could mistrigger the data-acquisition system before impact. The striker tube is launched by a spring system.

Since the axial stress–strain relations in the fiber are reduced from the lab measurements using one-dimensional wave propagation theory [23], all the components are aligned along a straight line on an optical table as shown in Fig. 15b. For measuring the elastic waves in the incident bar, while eliminating the effect of bending from impact, two high-resistance semiconductor strain gages (KYOWA KSP-2-1K-E4) are mounted in opposite positions of a circumference on the bar.

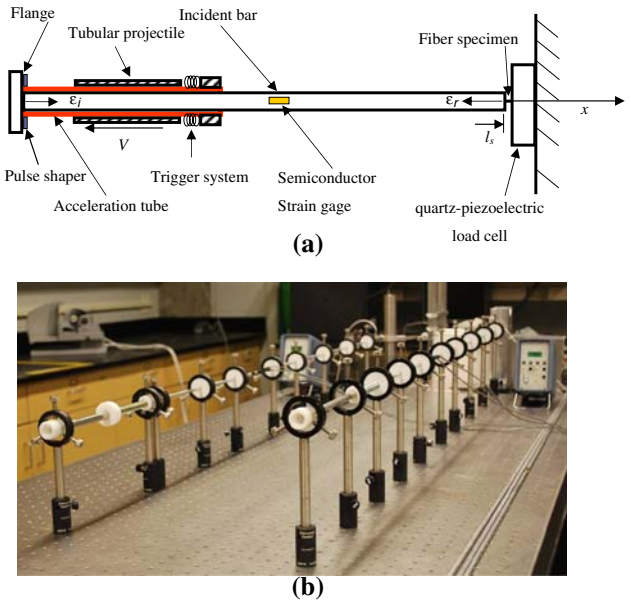

Fig. 15 The experimental setup of a miniature tension bar. **a** Schematic diagram. **b** A photograph

A fiber specimen with a short gage length of 2.5–10 mm is connected to the specimen end of the incident bar with an adhesive. The short gage length of the fiber specimen is to achieve an early dynamic force equilibrium state in the fiber specimen during deformation. The mounting arrangement for a single-fiber specimen [24, 25] is shown in Fig. 16. The two ends of the fiber specimen are glued to two small flat plates attached to the end surfaces of the incident bar and the force transducer. This method enables more accurate measurement of the gage length.

In this system, the transmission bar is replaced by a quartz–piezoelectric load cell (Kistler 9712B5) with a capacity of 22.24 N (5 lbf) since the transmitted force level is very low. The fiber's axial stress is calculated by

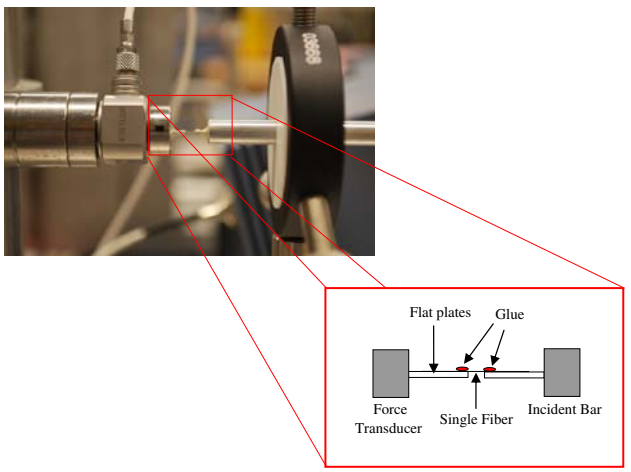

Fig. 16 The configuration of the mounting system for a single fiber experiment

dividing the measured force by the cross-sectional area of the fiber. Owing to the role of the cross-sectional area in the stress calculation, we measured the diameter of each fiber individually using a high-resolution SEM (Fig. 1). During an experiment on the modified Kolsky bar, the impact of the tubular striker on the flange generates a tensile incident stress wave that propagates toward the fiber specimen. When the stress wave arrives at the specimen, due to the small fiber specimen, most of the incident pulse is reflected back into the incident bar as the reflected pulse. The pulse that transmits through the specimen, which loads the specimen, eventually arrives at the load cell for recording. Since the specimen provides negligible resistance to the bar, the loading pulse needs to have a flat plateau to move the bar end at a constant velocity. The constant-velocity condition is needed to generate a constant strain rate in the specimen. The time histories of the raw strain and force signals obtained from such a dynamic experiment are shown in Fig. 17. The strain and force signals are recorded from the semiconductor strain gages mounted on the incident bar and from the quartz–piezoelectric load cell, respectively.

After the introduction of the D'Alembert solution, which is the general solution to the one-dimensional wave equation, the strain rate ($\dot{\varepsilon}$) and the strain (ε) of the fiber specimen are calculated using the following equations [23]:

$$\dot{\varepsilon} = -\frac{v}{l_s} = \frac{c_0}{l_s}(\varepsilon_i - \varepsilon_r) \tag{8}$$

where v is the particle velocity at the end of the incident bar, l_s is the length of the specimen, c_0 is the elastic bar wave velocity in the rod, and ε_i and ε_r are incident and reflected strains, respectively. By integration, we obtain the strain in the fiber specimen as a function of time t.

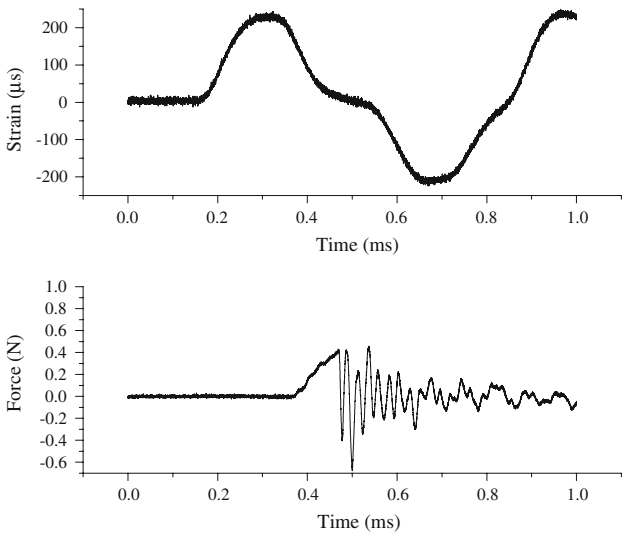

Fig. 17 Typical signals recorded from a miniature tension bar

$$\varepsilon = \int_0^t \frac{c_0}{l_s}(\varepsilon_i - \varepsilon_r)d\tau \quad (9)$$

Constant strain-rate deformation

A Kolsky bar experiment is typically designed to determine the rate effects on the material's stress–strain behavior. The specimen thus should deform nearly uniformly under an evenly distributed dynamic stress to provide valid stress–strain data. In order to delineate the rate effects, the specimen also needs to deform at a constant strain rate during one experiment. In a dynamic tension experiment on a fiber specimen, the shape of the reflected pulse is expected to be similar to that of the incident pulse (Eq. 1) due to weak resistance from a single fiber. Therefore, the constant strain rate deformation can be achieved by just controlling the shape of the incident pulse. A smooth and constant-amplitude incident pulse is obtained by adopting a copper alloy 110 foil with a thickness of 0.05 mm (0.002 in.) as a pulse shaper [26, 27]. The strain rate and strain histories in the fiber specimen during deformation are presented in Fig. 18, which indicate that the fiber deformed at a nearly constant strain rate owing to the modified shape of the incident pulse through the pulse shaper (Fig. 16).

Strain-rate effects

The experimental values of the longitudinal mechanical properties for the A265 fiber at the high strain rate are summarized in Table 3. Graphically, Figs. 19 and 20 show the distribution of tensile strength data of A265 fiber strength at high strain rates around 1000 s^{-1} obtained at two gage lengths of 2.5 and 10 mm. As a comparison, the strength data obtained quasi-statically are also displayed.

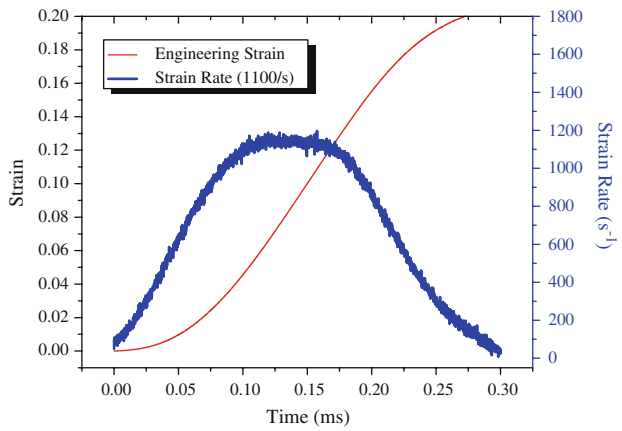

Fig. 18 Strain rate and strain histories in fiber specimen

Table 3 Longitudinal mechanical properties of A265 fibers at high strain rate

Gage length l (mm)	Tenacity (g/denier)	Ultimate strength (GPa)	Young's modulus (GPa)
2.5	50.47	6.41 ± 0.34	154.09 ± 8.34
10	40.78	5.18 ± 0.22	164.44 ± 11.19

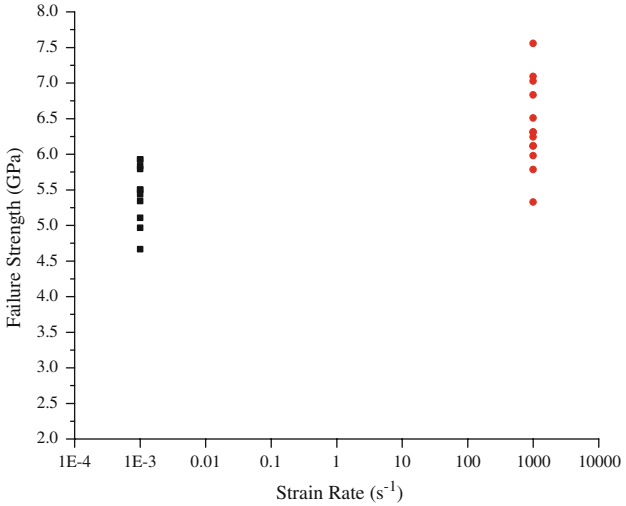

Fig. 19 Strain-rate effects of A265 single fibers at the gage length of 2.5 mm

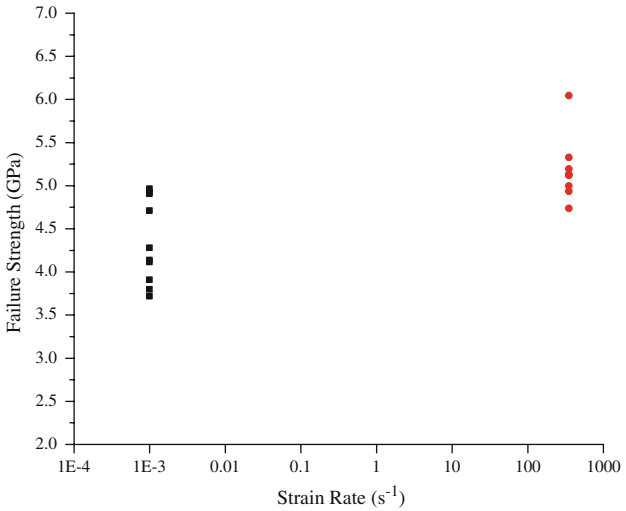

Fig. 20 Strain-rate effects of A265 single fibers at the gage length of 10 mm

As shown in Figs. 19 and 20, the average tensile strength of the A265 fiber increases by 16.6% when the strain rate is increased from quasi-static to dynamic. In a range of strains rate around 1000 s^{-1}, the failure strengths of A265 fibers are 6.41 ± 0.34 and 5.18 ± 0.22 GPa at the gage

lengths of 2.5 and 10 mm, respectively, as averaged from 15 experiments at each length. These results clearly show that the tensile strength of the fiber is both rate and gage-length dependent.

Conclusions

Experiments on single A265 fibers were performed to determine the mechanical properties of this high-performance fiber. Four elastic constants were obtained from longitudinal tensile tests, transverse compression tests, and torsional tests. Transverse Young's modulus (E_1), longitudinal Young's modulus (E_3), longitudinal shear modulus (G_{13}), and longitudinal Poisson's ratios (v_{31}) obtained are 1.83 GPa, 159.78 ± 3.21 GPa, 12.03 ± 0.78 GPa, and 0.402, respectively.

Quasi-static tensile tests were performed at five different gage lengths of 2.5, 5.5, 10, 50, and 100 mm. Experimental results show the dependence of the tensile strength of this fiber on gage length. The transverse compression experimental results in the large deformation range show the transverse compressive behavior of an A265 single fiber is nonlinear and pseudo-elastic. After few cycles of loading and unloading, a large residual strain (~25% nominal strain) remains in the fiber.

A miniature tension bar was used to investigate the strain-rate sensitivity of the fiber in its axial tensile behavior. The experimental results show that the behavior of a single A265 fiber is strain-rate sensitive. As the strain rate increases from $\dot{\varepsilon} = 0.001\,\mathrm{s}^{-1}$ to $\dot{\varepsilon} \approx 1000\,\mathrm{s}^{-1}$, the tensile strength increases by 16.6%. The high-rate experiments also confirm that the gage-length effects also exist in high-rate tensile strength data.

References

1. Yang HH (1992) Kevlar aramid fiber. John Wiley & Sons, New York, NY
2. Morton WE, Hearle JWS (1993) Physical properties of textile fibres. The Textile Institute, UK
3. Wang Y, Xia Y (1998) Compos Part A Appl Sci 29A:1411
4. Shim VPW, Lim CT, Foo KJ (2001) Int J Impact Eng 25:1
5. Creasy TS (2002) J Compos Mater 36:183
6. Languerand DL, Zhang H, Murthy NS, Ramesh KT, Sanoz F (2009) Mater Sci Eng A 500:216
7. Cheng M, Chen W (2005) J Eng Mater-T ASME 127:197
8. Kawabata S (1990) J Text Inst 81:432
9. Singletary J, Davis H, Ramasubramanian MK, Knoff W, Toney M (2000) J Mater Sci 35:573. doi:10.1023/A:1004764024568
10. Cheng M, Chen W, Weerasooriya T (2004) Int J Solids Struct 42:6215
11. Tsai CL, Daniel IM (1999) Exp Mech 39:284
12. Sirichaisit J, Young RJ (1999) Polymer 40:3421
13. Kitagawa T, Yabuki K, Young RJ (2001) Polymer 42:2101
14. Li CT, Tietz J (1985) J Am Ceram Soc 68(8):C202
15. Turek DE (1993) Polym Eng Sci 33(6):328
16. Hadley DW, Ward IM, Ward J (1965) Proc R Soc A 285(1401):275
17. Pinnock PR, Ward IM, Wolfe JM (1966) Proc R Soc A 291(1425):267
18. Phoenix SL, Skelton J (1974) Text Res J 44:934
19. McEwen E (1949) Philos Mag 40(303):454
20. Kolsky H (1949) Proc Phys Soc B 62:676
21. Gray G (2000) In: Kuhn H, Medlin D (eds) Classic split-Hopkinson pressure bar testing ASM handbook, vol 8. Material Park, OH
22. Gray G, Blumenthal WR (2000) In: Kuhn H, Medlin D (eds) Split-Hopkinson pressure bar testing of soft materials ASM handbook, vol 8. Material Park, OH
23. Karl FG (1975) Wave motion in elastic solids. Oxford University Press
24. Thomason JL, Kalinka G (2001) Compos Appl Sci Manuf 32:85
25. Meretz S, Auersch W, Marotzke C, Schulz E, Hampe A (1993) Compos Sci Technol 48:285
26. Frew DJ, Forrestal MJ, Chen W (2002) Exp Mech 42:93
27. Frew DJ, Forrestal MJ, Chen W (2005) Exp Mech 45:186